Microwave plasma interaction in a printed transmission line for a power limiting application: from surface-wave-sustained to leaky-wave-sustained discharge

Lucas Fuster, Romain Pascaud, Jérôme Sokoloff, Gerjan Hagelaar, Patrick Hoffmann, Olivier Pascal, Thierry Callegari

Microwave plasma interaction in a printed transmission line for a power limiting application : from surface-wave-sustained to leaky-wave-sustained discharge.

Lucas Fuster[1,2,3], Romain Pascaud[3], Jérôme Sokoloff[2], Gerjan Hagelaar[2], Patrick Hoffmann[1], Olivier Pascal[2] and Thierry Callegari[2]

[1]Commissariat à l'Energie Atomique et aux Energies Alternatives – Centre de Gramat, BP 80200 46500 Gramat – France
[2]LAPLACE, Université de Toulouse, CNRS, INPT, UPS, Toulouse, France
[3]ISAE-SUPAERO, Université de Toulouse, France

E-mail: `lucas.fuster@laplace.univ-tlse.fr`

August 2021

Abstract. The coupling between a microwave signal and a plasma discharge in a suspended microstrip transmission line is analytically studied. Maxwell's equations are solved in a 2D approximation to get the expressions of the electromagnetic field. The wave propagation in the guiding structure is first explored without plasma, and for several modes and frequencies. A unified characterization of the three different modes that can propagate at the interface between two dielectric media, namely the leaky waves, the pseudo-surface wave and the pure surface wave, is given in terms of of both wave vectors and electromagnetic field magnitude distribution. This analyze allow to conclude that the fundamental mode in this case is a pseudo-surface wave. Thereafter, we focus on the microwave propagation with a uniform plasma inside the guiding structure. In the non collisional limit, it appears that the plasma discharge is sustained by the so-called pure surface wave, whereas in the collisional limit, a leaky wave propagates along the plasma column. Finally, a non-uniform density profile is taken into account in the calculation. The numerical results obtained from the self-consistent simulation of the microwave-plasma coupling, in a previous work, are thus analyzed with the aid of the analytical formulas to identify the microwave coupling involved in our plasma-based microwave power limiter. The computed propagation constant from numerical data confirmed the type of coupling exhibited for a uniform electron density. Furthermore, we highlight the role of the dielectric slab, from which electromagnetic power transfer occurs into the plasma discharge.

Submitted to: *Plasma Sources Sci. Technol.*

1. Introduction

Microwave plasma sources can be used for a wide range of applications in chemistry, energy, and for sustainable development, to name but a few [1, 2]. They offer many advantages, such as high electron temperature, a wide range of working pressure, and no electrodes. Microwave discharges are usually generated by standing or propagating microwaves [1, 3].

Resonant cavities were one of the first microwave devices to generate plasma discharges [4]. At the resonance frequency, the microwave electric field is reinforced by creating standing waves within the cavity, that is to say the plasma chamber. This locally intensified electric field then enables microwave breakdown of the gas. This type of discharge is generally localized in space, and its size highly depends on the wavelength of the microwave signal.

Discharges with larger dimensions compared to the wavelength can also be obtained with guided microwave power. These travelling-wave discharges include surface wave sustained discharges (SWD), slow wave sustained discharges, or slot antenna type plasma sources (SLAN), for instance [3]. Although developed with the same objectives in mind, the coupling between microwave power and plasma can be quite different in these sources, but its understanding is essential for optimizing them.

For instance, the pioneering theoretical and experimental work of Trievelpiece and Gould [5] on the microwave propagation along cylindrical plasma columns has led to the successful development of surface wave sustained discharges (SWD) in dielectric tubes [6, 7]. The concept has since been extended to planar structures by Komachi *et al.*, in which plasma discharges are sustained in wide chambers with microwaves travelling along a grounded dielectric slab [8–10].

Recently, the authors have proposed a microstrip transmission line device integrating a microwave-sustained discharge for power limiting applications [11]. Although initially developed to protect against high-power microwave (HPM) threats, this device can also be seen as a potential microwave plasma source. It consists of a multilayer structure made up of two parallel planar conductors, between which there is a dielectric slab and a cavity filled with Argon at 10 Torr where the microwave plasma is generated and sustained. A first step has been reached in our previous work [11] where a self-consistent simulation of the interaction between the microwave signal and the plasma discharge was proposed. The numerical results were in good agreement with experimental ones, both in terms of plasma dynamics and microwave power ratios. For instance, we demonstrated a limitation threshold of 28 dBm and time responses of 25 μs for this absorptive microwave power limiter with more than 60 % of the microwave input power absorbed by the plasma.

If interesting performances have already been achieved at 3 GHz, this device still requires an understanding of the coupling between the microwave power and the plasma to optimize it.

The existing interface between the dielectric slab and the microwave-sustained plasma in our device suggests similarities with other types of travelling-wave discharges. Considering a semi-infinite elastic medium, Lord Rayleigh discovered that a source of finite dimensions can excite two kinds of waves, "space waves" that propagate in all directions, and "surface waves" that propagate along the boundary [12]. If we restrict ourselves to the case of a semi-infinite lossless dielectric slab bounded with vacuum, it is well known that three types of waves can propagate along the dielectric interface:

- the pure surface waves or surface plasmons [13] that have an evanescent electromagnetic field on both sides of the boundary, and for which the wave vectors in both media are collinear to the interface [14],
- the pseudo-surface waves that have an electromagnetic field evanescent in vacuum only, and for which the wave vector is only collinear to the interface in vacuum,
- the leaky waves (also denoted as space waves, radiation waves, or partially guided waves in the literature) that have an electromagnetic field that consists of volume waves on both sides of the interface [15].

It seems that the plasma community discriminates these modes in terms of the spatial distribution of the electromagnetic field magnitude [15–18], whereas the microwave and antennas communities do it in terms of wave vectors that describes the propagation of phase planes [14, 19, 20].

In this paper, we present an analytical study of the interaction between microwave and plasma in the suspended microstrip transmission line introduced in [11]. Maxwell's equations are solved in a 2D approximation to get the expressions of the electromagnetic field within this specific device. The wave propagation in the guiding structure is first explored without plasma, and for several modes and frequencies. It gives a unified description in terms of both wave vectors and electromagnetic field magnitude distribution for the specific types of waves that can be encountered. Thereafter, we focus on the microwave propagation with a uniform plasma inside the guiding structure. Finally, a non-uniform density profile is taken into account in the calculation. The numerical results obtained from the self-consistent simulation

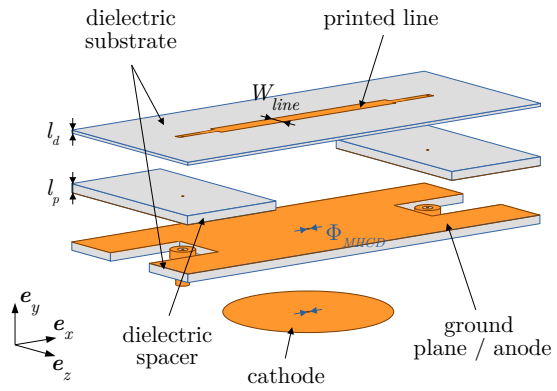

Figure 1. Exploded 3D view of the plasma-based microwave power limiter in suspended microstrip technology.

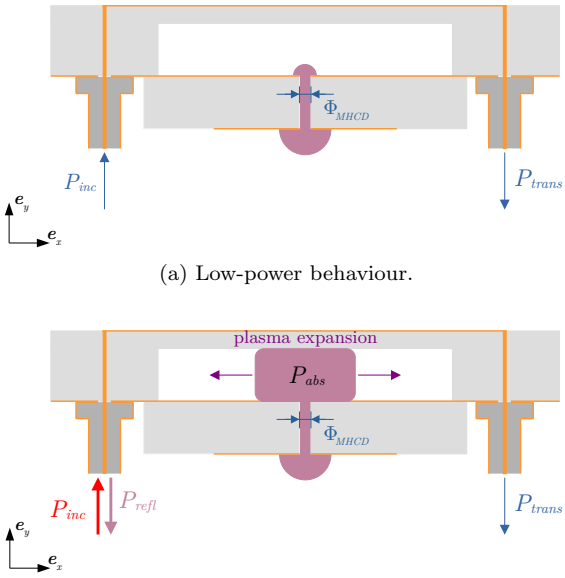

(a) Low-power behaviour.

(b) High-power behaviour.

Figure 2. Principle of operation of the plasma-based microwave power limiter in suspended microstrip technology.

of the microwave-plasma coupling in our previous work [11], are thus analyzed with the aid of the analytical formulas in order to identify the microwave coupling involved in our plasma-based microwave power limiter.

2. Problem and general solution

2.1. Principle of operation

The exploded view of the plasma-based microwave power limiter is shown in figure 1. It consists of a suspended microstrip transmission line in which a cavity is machined to accomodate a low pressure gas. This cavity is located between the two line conductors, the ground plane and the printed line. Note that a direct current (DC) micro-hollow cathode discharge (MHCD) is also used to produce seed electrons within the cavity, that help to reduce the microwave breakdown threshold for the power limiter. The operating principle of this device is described in detail in [11], and it is here briefly recalled.

When a microwave signal propagates along the suspended microstrip transmission line, namely along the x-direction, the electric field is mostly confined between the two conductors. If it is a low-power signal (see figure 2a), almost all the incident power is transmitted through the device with very low insertion loss of 0.2 dB. However, if the microwave power is large enough, gas breakdown may be ignited and expand into the low pressure gas-filled cavity (see figure 2b). This microwave-sustained plasma then absorbs and/or reflects the incoming signal thereby reducing the output power of the device. It is important to point out that the MHCD, which remains switched on throughout the operation, only plays a starter role at the beginning and does not contribute to the plasma expansion inside the cavity (the MHCD can be switched off without any consequence).

In our previous work [11], this device has been widely studied experimentally in terms of both plasma dynamics and steady-state microwave power ratios. These results have been compared to numerical ones obtained from the self-consistent simulation of the interaction between the microwave field and the plasma discharge, and a good agreement was obtained between these two approaches. Here, we use this simulation code to compute several quantities that characterize the plasma such as its electron density, the electromagnetic field within it, or the Poynting vector distribution in the transmission line. These numerical results are then used as input data to the following analytical developments in order to understand the way the microwave field couples to the discharge.

2.2. Problem geometry for the analytical model

The dimensions of the suspended microstrip transmission line are $W_{line} = 8$ mm, $l_d = 0.508$ mm, and $l_p = 1.524$ mm to achieve a 50 Ω characteristic impedance. It thus has a large width-to-height ratio $W_{line}/(l_d + l_p)$ of 3.9, and fringing effects can be neglected. As shown in figure 3, the central longitudinal part of the suspended microstrip transmission line can be seen as an inhomogeneous dielectric filled parallel-plate waveguide [21]. Finally, the only notable difference with the structure mentioned in the introduction, namely the semi-infinite dielectric slab bounded with vacuum, is the presence of an electric conductor, the transmission line ground plane at $y = -l_p$.

The relative permittivity of the dielectric sub-

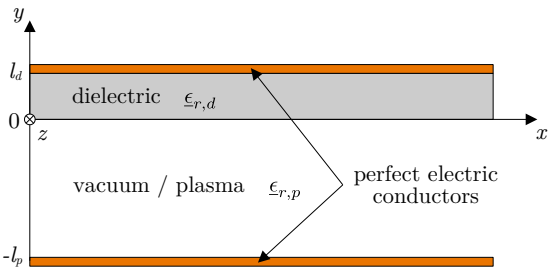

Figure 3. Schematic of the plasma-based microwave power limiter in suspended microstrip technology.

strate layer, or slab, is fixed to $\underline{\varepsilon}_{r,d} = 3.55$. The dielectric losses are thus neglected in the remainder of this work. Within the cavity, we consider either the relative permittivity of the vacuum in the absence of plasma, $\underline{\varepsilon}_{r,p} = 1$, or the relative permittivity given by the Drude model in the presence of plasma [18]

$$\underline{\varepsilon}_{r,p} = 1 - \frac{\omega_{pe}^2}{\omega^2 + \nu_m^2} + i\frac{\nu_m}{\omega}\frac{\omega_{pe}^2}{\omega^2 + \nu_m^2} \tag{1}$$

with ν_m the momentum transfer frequency of collisions with the gas, ω the microwave angular frequency, and ω_{pe} the electron plasma angular frequency

$$\omega_{pe} = \sqrt{\frac{n_e e^2}{m_e \varepsilon_0}} \tag{2}$$

where n_e, e, m_e, and ε_0 are respectively the electron density, the Coulomb charge, the electron mass, and the vacuum permittivity.

2.3. Solutions to Maxwell's equations

The problem depicted in figure 3 is a typical boundary-value problem associated with guided wave propagation in waveguides [22]. Its solutions constitute an infinite set of waveguide modes of the transverse electric (TE) and transverse magnetic (TM) type, characterized by the presence of longitudinal magnetic or electric field components, respectively.

In the following developments, as in [11], we are interested in the fundamental TM mode and some higher-order ones for which the electromagnetic field derives, in a free source space, with a temporal dependence in $e^{-i\omega t}$ and considering the Lorenz gauge, from the magnetic vector potential $\underline{\boldsymbol{A}}_m = \underline{\Psi}_m(y)\mathrm{e}^{i\underline{k}_x x}\mathbf{e}_x$ and the following equation [23]

$$\boldsymbol{\Delta}\underline{\boldsymbol{A}}_m + \underline{k}_m^2\underline{\boldsymbol{A}}_m = 0 \tag{3}$$

where m denotes the medium, with $m = p$ for the plasma or the vacuum, and $m = d$ for the dielectric. The constant $\underline{k}_m = k_0\sqrt{\underline{\varepsilon}_{r,m}}$ (with $k_0 = \omega/c$ the wave number in the vacuum) is the norm of the wave vector $\underline{\boldsymbol{k}}_m$ defined as

$$\underline{\boldsymbol{k}}_m = \underline{k}_x\,\mathbf{e}_x + \underline{k}_{y,m}\,\mathbf{e}_y \tag{4}$$

that leads to the relation

$$k_0^2\underline{\varepsilon}_{r,m} = \underline{k}_x^2 + \underline{k}_{y,m}^2 \tag{5}$$

with $\underline{k}_x$ the propagation constant to be determined, that is the same in both media since the matching conditions for the electromagnetic field at the interface have to be verified whatever the position x considered. Equation (3) is then solved with perfect electric conductor boundary conditions at the metal boundaries (*i.e.*, at $y = l_d$ and $y = -l_p$), for which the electric field is normal to the conductor.

Knowing $\underline{\boldsymbol{A}}_m$, the expressions of the electric and magnetic fields can be determined in each medium using

$$\underline{\boldsymbol{E}}_m = i\frac{\omega}{\underline{k}_m^2}\left[\boldsymbol{\nabla}(\boldsymbol{\nabla}\cdot\underline{\boldsymbol{A}}_m) + \underline{k}_m^2\underline{\boldsymbol{A}}_m\right] \tag{6}$$

$$\underline{\boldsymbol{B}}_m = \boldsymbol{\nabla}\times\underline{\boldsymbol{A}}_m. \tag{7}$$

The solutions in the dielectric slab and in the plasma (or the vacuum) can be written as

$$\underline{E}_d^x(x,y) = iE_0\frac{\underline{\varepsilon}_{r,p}}{\underline{\varepsilon}_{r,d}}\frac{\underline{k}_{y,d}}{\underline{k}_x}\frac{\sin(\underline{k}_{y,d}[l_d - y])}{\cos(\underline{k}_{y,d}l_d)}\mathrm{e}^{i\underline{k}_x x} \tag{8}$$

$$\underline{E}_d^y(x,y) = E_0\frac{\underline{\varepsilon}_{r,p}}{\underline{\varepsilon}_{r,d}}\frac{\cos(\underline{k}_{y,d}[l_d - y])}{\cos(\underline{k}_{y,d}l_d)}\mathrm{e}^{i\underline{k}_x x} \tag{9}$$

$$\underline{B}_d^z(x,y) = E_0\frac{k_0^2\underline{\varepsilon}_{r,p}}{\omega\underline{k}_x}\frac{\cos(\underline{k}_{y,d}[l_d - y])}{\cos(\underline{k}_{y,d}l_d)}\mathrm{e}^{i\underline{k}_x x} \tag{10}$$

and

$$\underline{E}_p^x(x,y) = -iE_0\frac{\underline{k}_{y,p}}{\underline{k}_x}\frac{\sin(\underline{k}_{y,p}[y + l_p])}{\cos(\underline{k}_{y,p}l_p)}\mathrm{e}^{i\underline{k}_x x} \tag{11}$$

$$\underline{E}_p^y(x,y) = E_0\frac{\cos(\underline{k}_{y,p}[y + l_p])}{\cos(\underline{k}_{y,p}l_p)}\mathrm{e}^{i\underline{k}_x x} \tag{12}$$

$$\underline{B}_p^z(x,y) = E_0\frac{k_0^2\underline{\varepsilon}_{r,p}}{\omega\underline{k}_x}\frac{\cos(\underline{k}_{y,p}[y + l_p])}{\cos(\underline{k}_{y,p}l_p)}\mathrm{e}^{i\underline{k}_x x} \tag{13}$$

Finally, the propagation constant $\underline{k}_x$ is determined by matching the longitudinal components of the electric field at the interface between the dielectric slab and the cavity. It leads to the following transcendental equation [23]

$$-\frac{\underline{k}_{y,p}}{\underline{\varepsilon}_{r,p}}\tan(\underline{k}_{y,p}l_p) = \frac{\underline{k}_{y,d}}{\underline{\varepsilon}_{r,d}}\tan(\underline{k}_{y,d}l_d) \tag{14}$$

This equation can easily be solved numerically. In the low frequency limit, for which $|\underline{k}_{y,d}l_d| \ll 1$ and $|\underline{k}_{y,p}l_p| \ll 1$, note that it leads to the following equation for the propagation constant [21]

$$\underline{k}_x = k_0\sqrt{\frac{\underline{\varepsilon}_{r,d}\underline{\varepsilon}_{r,p}}{\underline{\varepsilon}_{r,d}l_p + \underline{\varepsilon}_{r,p}l_d}(l_d + l_p)} \tag{15}$$

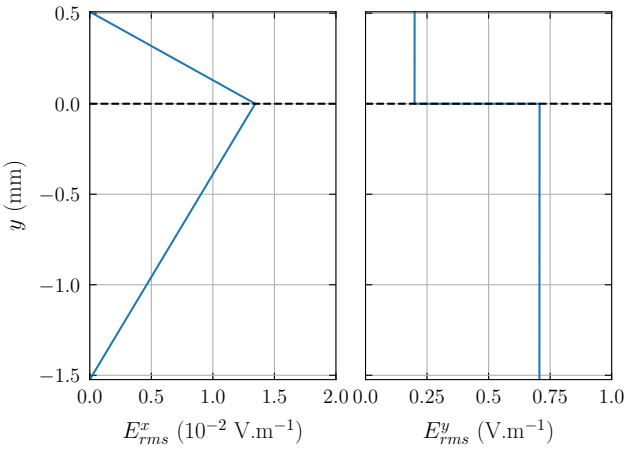

Figure 4. Profiles of the RMS values of the E^x and E^y electric field components in the y-direction for the fundamental mode at 3 GHz and for an arbitrary magnitude $E_0 = 1$ V.m^{-1}. The dotted black line represents the boundary between the dielectric slab and the vacuum.

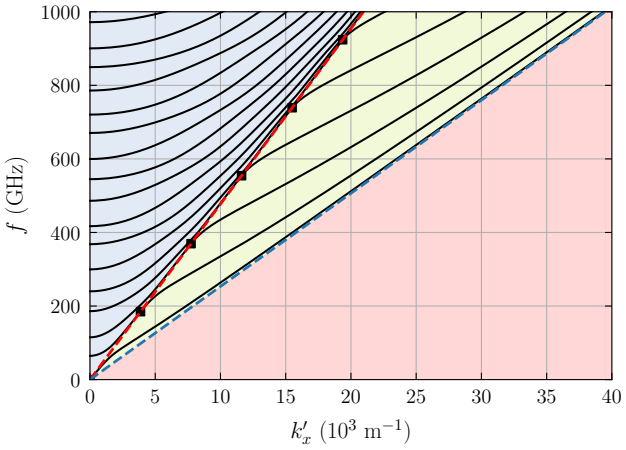

Figure 5. Dispersion diagram of the TM modes for the empty line with $l_d = 0.508$ mm, $l_p = 1.524$ mm, and $\underline{\varepsilon}_{r,d} = 3.55$. TM modes are represented by the black lines, the vacuum light cone $k'_x = k_0$ by the red dashed line, and the dielectric light cone of equation $k'_x = k_0\sqrt{\underline{\varepsilon}_{r,d}}$ by the blue dashed line. Blue region identifies leaky-wave alike modes, green region pseudo-surface-wave alike modes, and red region surface plasmons.

3. Propagating modes in the lossless empty waveguide

We first discuss the modal analysis of the proposed device considering the cavity without plasma [21]. In other words, it means that $\underline{\varepsilon}_{r,p} = 1$ in the previous developments.

3.1. Fundamental mode in the low-frequency limit

The fundamental, or dominant, mode characteristics in the low-frequency limit are computed assuming a signal frequency of 3 GHz and an arbitrary magnitude $E_0 = 1$ V.m^{-1}. This is the operating frequency selected during previous tests of the microwave power limiter [11].

The profiles of the root mean square (RMS) values of the associated E^x and E^y electric field components in the y-direction are shown in figure 4. As expected, they verify the matching of the longitudinal electric field component and of the perpendicular component of the electric displacement field ($\underline{\boldsymbol{D}}_m = \underline{\varepsilon}_{r,m}\underline{\boldsymbol{E}}_m$) at the interface. Moreover, we observe the expected electric field distribution for a quasi-transverse electromagnetic (TEM) mode [21]. Indeed, if we still have rigorously a TM mode, the RMS amplitude of the longitudinal E^x electric field component is 53 times less than the amplitude of the E^y component. The inhomogeneous dielectric filled parallel-plate waveguide may be analyzed as a transmission line in that case.

At higher frequency, however, the mode of propagation departs from a quasi-TEM mode. In order to discuss such complex electromagnetic field distribution, to identify and to characterize the three different types of propagation that can exist in the microstrip line, we then focus on the higher-order modes of this waveguiding structure that appear at much higher frequencies than 3 GHz for the empty line.

3.2. Higher-order modes

The transcendental equation (14) is numerically solved to find all the TM eigenmodes associated with this waveguide in the frequency range from 0 to 1 THz. Of course, such a frequency range largely covers the range of interest in this work, but it allows us to observe the behaviour of several higher-order modes, and to point out their electromagnetic field distributions. Note that since we focus on the lossless empty waveguide, the propagation constant is real and $\underline{k}_x = k'_x$.

The resulting dispersion diagram is shown in figure 5. The TM modes are represented by the black lines, the vacuum light cone of equation $k'_x = k_0$ by the red dashed line, and the dielectric light cone of equation $k'_x = k_0\sqrt{\underline{\varepsilon}_{r,d}}$ by the blue dashed line. These two light cones divide the dispersion diagram into three regions. As we shall see, these identify the three types of waves encountered at the dielectric interface, and discussed in the introduction: leaky waves (*i.e.*, wave leaking from the dielectric slab), pseudo-surface waves, and surface plasmons.

Let's consider the first higher-order mode that has a cut-off frequency equal to 64.5 GHz. As observed in figure 5, its dispersion curve crosses the first light cone (*i.e.*, $k'_x = k_0$) at 184.78 GHz, while it never crosses the second one (*i.e.*, $k'_x = k_0\sqrt{\underline{\varepsilon}_{r,d}}$). One can analyze each side of its dispersion curve by looking to the field distribution of the mode. To do this, we can first focus

on the $\underline{E}_p^y$ component of the electromagnetic field.

When $k'_x \leq k_0$, $\underline{k}_{y,p}$ is purely real (*i.e.*, $\underline{k}_{y,p} = k'_{y,p}$), and $\underline{E}_p^y$ can be rewritten as

$$\underline{E}_p^y(y,z) = \frac{E_0}{2\cos(k'_{y,p}l_p)}\mathrm{e}^{i\left(k'_x x + k'_{y,p}[y+l_p]\right)} + \frac{E_0}{2\cos(k'_{y,p}l_p)}\mathrm{e}^{i\left(k'_x x - k'_{y,p}[y+l_p]\right)} \tag{16}$$

and the electromagnetic field in the plasma region can be seen as a superposition of two plane waves $\mathcal{E}_p^+$ and $\mathcal{E}_p^-$ that both propagate in the x-direction, and in opposite directions along the y-direction [14, 20].

When $k'_x > k_0$, the constant $\underline{k}_{y,p}$ becomes purely imaginary (*i.e.*, $\underline{k}_{y,p} = ik''_{y,p}$) and the $\underline{E}_p^y$ component then writes

$$\underline{E}_p^y(y,z) = E_0\frac{\cosh(k''_{y,p}[y+l_p])}{\cosh(k''_{y,p}l_p)}\mathrm{e}^{ik'_x x} \tag{17}$$

where the amplitude in factor of $\mathrm{e}^{ik'_x x}$ decreases from the interface to the ground plane, as fast as $k''_{y,p}$ is high. In this case, the electromagnetic field reduces to a single inhomogenous plane wave $\mathcal{E}_p^{evan.}$ that only propagates along the x-direction and is evanescent in the y-direction. Such analyses can also be conducted for the electromagnetic field in the dielectric slab, but since $k'_x < k_0\sqrt{\underline{\varepsilon}_{r,d}}$, we only have to consider the equivalent of equation (16) whatever the frequency.

This way of representing the problem provides a very interesting tool for understanding propagation mechanisms in the waveguide depending on the frequency of the wave. Indeed, whathever the expression considered, the arguments in the exponential can be rewritten as a function of the variable ϕ_m defined as

$$\phi_m = \int \boldsymbol{k}'_m \cdot \mathrm{d}\boldsymbol{r} \tag{18}$$

with $\mathrm{d}\boldsymbol{r} = \mathrm{d}x\mathbf{e}_x + \mathrm{d}y\mathbf{e}_y$ and $\boldsymbol{k}'_m = k'_x\mathbf{e}_x + k'_{y,m}\mathbf{e}_y$ the real part of the wave vector in the medium m. The variable ϕ_m is part of the eikonal equation from geometric optics that describes the propagation of optical rays

$$\boldsymbol{\nabla}\phi_m = k_0 n_m \boldsymbol{u} \tag{19}$$

with $n_m = \sqrt{\varepsilon_{r,m}}$ the refractive index of the medium m, and $\boldsymbol{u}$ the unit vector which provides the local direction of the ray. Note that since the media are homogeneous, we simply have $\boldsymbol{\nabla}\phi_m = \boldsymbol{k}'_m$ in our case. Thus, the evolution of a ray obtained for the first higher-order mode is shown in figure 6 for several frequencies between 85 and 300 GHz. We recall that the crossing of the light cone occurs at 184.78 GHz in that case.

Let's first discuss the path of a ray at 85 GHz. A ray, whose history we do not know, starts from point A located on the upper perfect electric conductor, namely the line. It then propagates to point B on the dielectric interface, that is to say the dioptre. There, it is partly reflected and refracted. The reflected ray then travels from point B to point C on the line, where it is totally reflected. The refracted ray in the cavity propagates to point D on the lower perfect electric conductor, the ground plane, where it is also totally reflected. Signal propagation in the line is therefore the result of a succession of reflections from the perfectly electric conducting planes, and refractions by the dioptre.

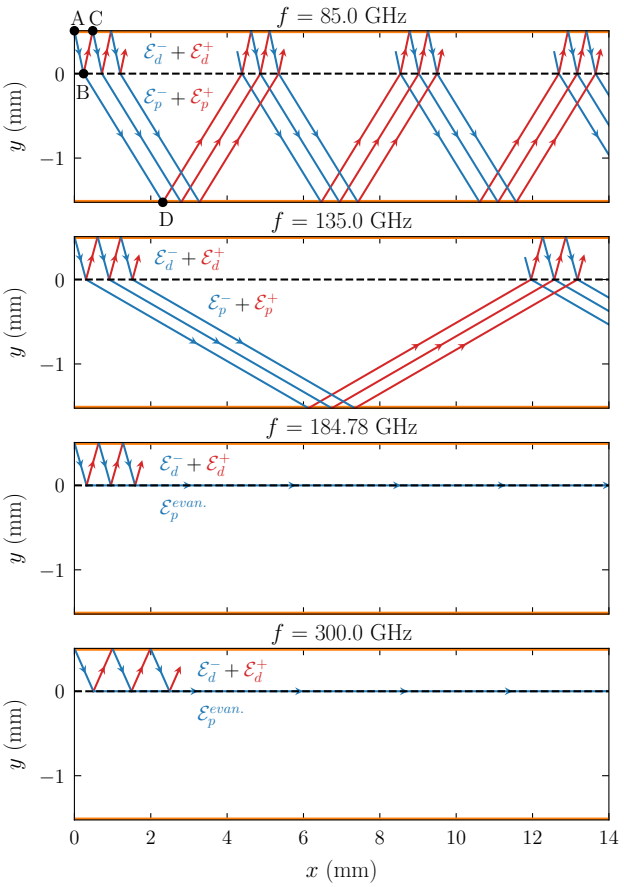

Figure 6. Schematic illustrating the path of a ray for the first higher-order mode and for several frequencies.

We note in figure 6 that, as the frequency increases up to 135 GHz, for instance, the rays refracted in the cavity form a smaller angle with the dielectric interface. This evolution obviously follows the Snell-Descartes laws of geometrical optics [24] (see Appendix A for the demonstration). Since we are studying the case of the empty cavity with $\underline{\varepsilon}_{r,p} = 1$, we have the refraction index $n_p = \sqrt{\underline{\varepsilon}_{r,p}} = 1$, and thus the following expression for the angle of refraction i_p

$$i_p = \arcsin\left(\frac{k'_x}{k_0}\right) \tag{20}$$

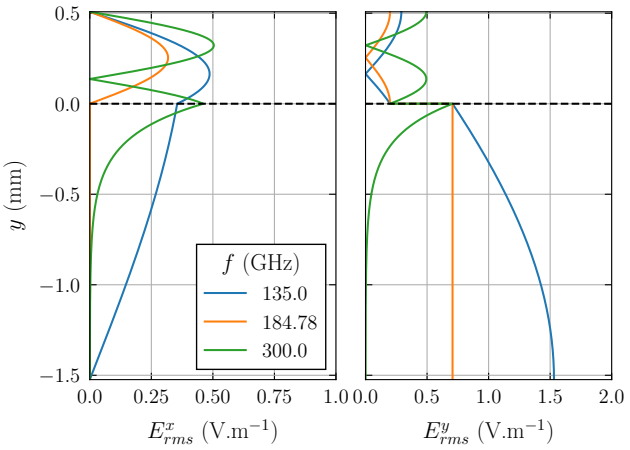

Figure 7. Profiles of the RMS values of the E^x and E^y electric field components in the y-direction for the first higher-order mode at different frequencies and for an arbitrary magnitude $E_0 = 1$ V.m^{-1}. The dotted black line represents the boundary between the dielectric slab and the vacuum.

When dispersion curve of this higher-order mode crosses the red dashed line in figure 5, that is to say for $f = 184.78$ GHz, the real part of i_p in equation (20) is equal to $\pi/2$. It is the critical angle and we observe total internal reflection in the dielectric slab, as used in optical fibers, for instance [24]. The ray is then confined in the dielectric slab while propagating. Note that for larger frequencies, for instance 300 GHz in figure 6, the propagation mechanism remains the same.

Finally, the RMS values of the E^x and E^y components in the y-direction are shown in figure 7 for the first higher-order mode. For frequencies such that $k'_x < k_0$ (*i.e.*, 135 GHz or the blue region in figure 5), the profile takes the form of cosine arcs in each medium, representing the interference between the two plane waves constituting the field. However, when k'_x exceeds k_0 (*i.e.*, 300 GHz or the green region in figure 5), the electric field becomes evanescent in the cavity.

This study of the propagation mechanisms through the wave vector components and electric field profiles helps identify the different types of waves involved in this waveguide.

3.3. Discussion

As shown in figure 5, three regions can be distinguished in the dispersion diagram. They correspond to the three types of wave propagation encountered when dealing with a semi-infinite lossless dielectric slab bounded with vacuum, and already mentioned in the introduction. It is important to note that, in our case, the waveguiding structure also includes two perfect electric conductors in addition to the dielectric slab.

The blue region corresponds to leaky waves. The optical ray is generated by a wave vector for which $k'_{y,d} \neq 0$, $k'_{y,p} \neq 0$, and the field is not evanescent either in the cavity or in the dielectric slab. Strictly speaking, these are not exactly leaky waves since the lower perfect electric conductor plate prevents them from radiating out to infinity. The electromagnetic wave is thus reflected towards the dielectric slab and no attenuation is observed as the wave propagates along the x-direction.

The green region corresponds to pseudo-surface waves, for which the signal is guided in the dielectric slab only. The optical way is generated by a wave vector for which $k'_{y,d} \neq 0$, $k'_{y,p} = 0$, and $k''_{y,p} > 0$. This last condition demonstrates the evanescent nature of the field within the cavity.

Finally, the red region corresponds to pure surface waves for which $k'_{y,d} = 0$, $k''_{y,d} > 0$, $k'_{y,p} = 0$, and $k''_{y,p} > 0$. The field is then evanescent on both sides of the dielectric interface. As shown in figure 5, the dispersion curves of the modes do not cross the dielectric light cone whatever the frequency, and as a result, this pure surface wave can not exist in the empty waveguide. The conditions of appearance of such a mode will be discussed in the next section.

A few comments can be made in the light of these results.

First of all, the general criterion to identify surface waves used by the plasma community, namely an electric field that is evanescent or not, is valid as long as the evanescence is not a consequence of power absorption, namely if the medium in which the evanescence is observed is lossless. Thus, as we will discuss in the next section, the criterion mentioned above is valid in the presence of a non-collisional plasma, that is to say if the electron momentum transfer frequency ν_m is negligible compared to the wave angular frequency ω. In that case, the decay of the electromagnetic field is related to the physical mechanisms described above for surface waves.

When the plasma is collisional, however, the decay of the fields is also partially due to the collisional absorption of the electromagnetic power by the electrons. These are typically our conditions of operation, namely a frequency of 3 GHz and a pressure of 10 Torr of Argon. The general criterion can thus no longer be used, and the identification has to rely on the wave vectors properties. Note that this clarification does not invalidate the researches on SWD since most of these works have been conducted for plasmas at very low pressure (*i.e.*, around 10 mTorr) and for frequencies typically around 2.45 GHz.

The description of the wave propagation given above only considers one of the two plane waves in equation (16). Since the electromagnetic field is the superposition of these two plane waves of equal

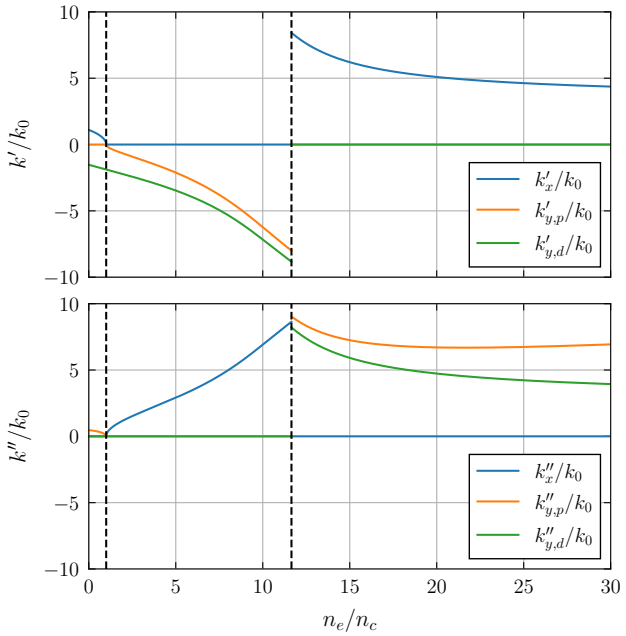

Figure 8. Real and imaginary parts of $\underline{\boldsymbol{k}}_d/k_0$ and $\underline{\boldsymbol{k}}_p/k_0$ as a function of the electron density n_e normalized to the critical density $n_c = 1.12 \times 10^{17}$ m^{-3} at 3 GHz for a non-collisional plasma (*i.e.*, $\nu_m = 0$). The vertical black dashed lines stand for the electron densities $n_e = n_c$ and $n_e = \left(1 + \varepsilon'_{r,d}\frac{l_p}{l_d}\right) n_c$.

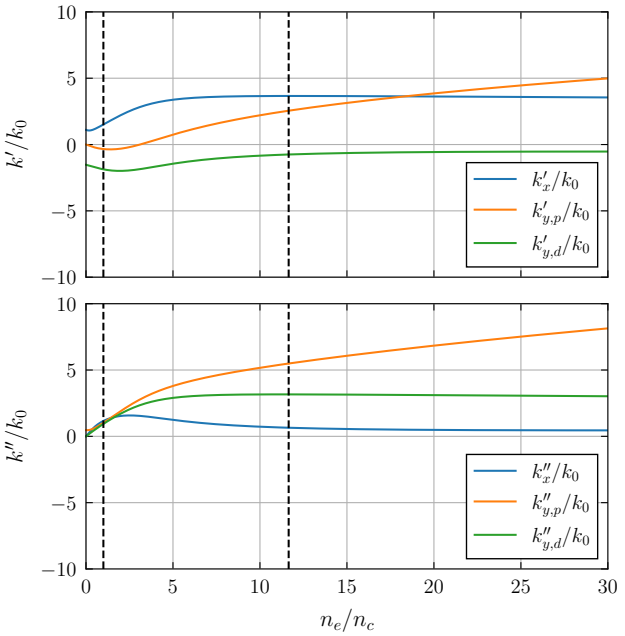

Figure 9. Real and imaginary parts of $\underline{\boldsymbol{k}}_d/k_0$ and $\underline{\boldsymbol{k}}_p/k_0$ as a function of the electron density n_e normalized to the critical density $n_c = 9.94 \times 10^{17}$ m^{-3} at 3 GHz for a collisional plasma (*i.e.*, $\nu_m = 5.3 \times 10^{10}$ s^{-1}). The vertical black dashed lines stand for the electron densities $n_e = n_c$ and $n_e = \left(1 + \varepsilon'_{r,d}\frac{l_p}{l_d}\right) n_c$.

magnitudes, the effective wave vector associated to the total field is directed only along the x-direction, and the magnitude of this wave vector is equal to the propagation constant k'_x.

Finally, the classification in terms of wave vector components allows to assimilate the fundamental mode, described as a quasi-TEM mode in the literature, to a pseudo-surface wave.

4. Fundamental mode in the waveguide filled with homogeneous plasma

We now study the fundamental mode considering that the cavity is fully filled with an homogeneous plasma described by the Drude model given by equation (1).

4.1. Non-collisional plasma

Let's first assume that the plasma is non-collisional such that $\nu_m = 0$, or at least $\nu_m/\omega \ll 1$. The components of the wave vectors in the dielectric slab and in the plasma are thus given in figure 8 as a function of the plasma density normalized to the critical density, for a frequency of 3 GHz. Note that the critical density is equal to 1.12×10^{17} m^{-3} in that case. Three types of propagation can be distinguished.

- For $0 < n_e < n_c$, that is to say for $1 > \underline{\varepsilon}_{r,p} > 0$, we have $k'_{y,d} \neq 0$ and $k'_{y,p} = 0$. The real part of the wave vectors is parallel to the interface inside the plasma, but not in the dielectric slab. It is therefore a pseudo-surface wave as described in Section 3.3.
- For $n_c < n_e < \left(1 + \varepsilon'_{r,d}\frac{l_p}{l_d}\right) n_c$, that is to say for $0 > \underline{\varepsilon}_{r,p} > -\varepsilon'_{r,d}\frac{l_p}{l_d}$, we have a cut-off regime for which the propagation constant $\underline{k}_x$ is purely imaginary, which means that no propagation is possible in the waveguide.
- For $\left(1 + \varepsilon'_{r,d}\frac{l_p}{l_d}\right) n_c < n_e$, that is to say for $\underline{\varepsilon}_{r,p} < -\varepsilon'_{r,d}\frac{l_p}{l_d}$, the real part of the wave vectors are directed along the x-direction at the dielectric interface in both media. It is a pure surface wave, as in surface wave sustained discharges.

4.2. Collisional plasma

In our microwave power limiter, the cavity is filled with Argon at 10 Torr. The momentum transfer frequency can thus be approximated by $\nu_m = 5.3 \times 10^{10}$ s^{-1} [25], and the resulting plasma is no longer non-collisional at 3 GHz since $\nu_m/\omega = 2.8$.

The components of the wave vectors for these conditions are shown in figure 9 as a function of the

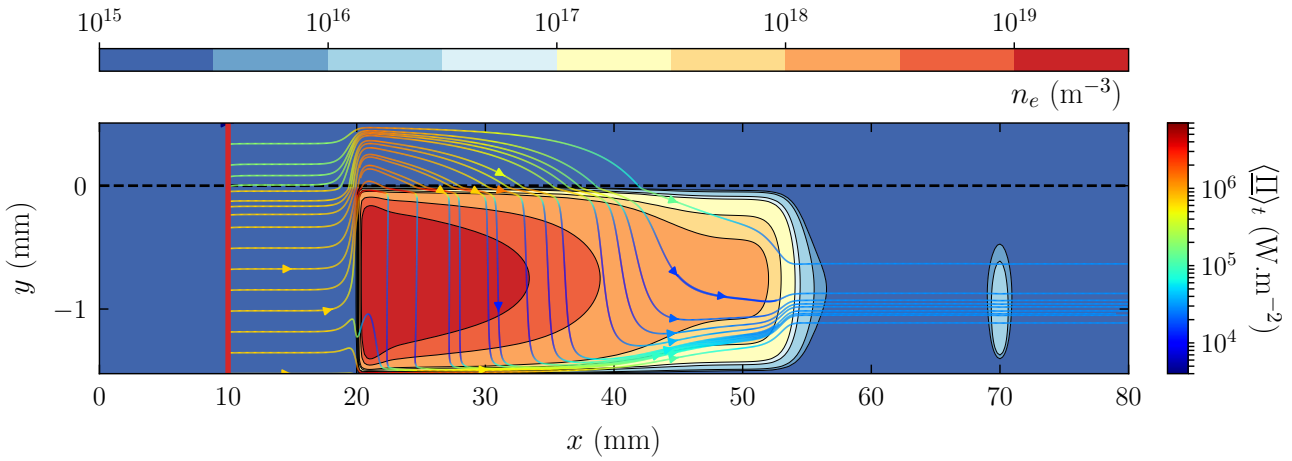

Figure 10. Simulated time-average Poynting vector lines and electron density for a steady-state plasma with an incident power of 10 W at 3 GHz. The dotted black line marks the dielectric slab and the plasma. The red line at $x = 10$ mm represents the current sheet that generates the incident electromagnetic field [11].

electron density normalized to the critical density at 3 GHz. Note that the critical density‡ is now equal to 9.94×10^{17} m^{-3} at 3 GHz, which is slightly higher than for the non-collisional case. We can observe that there is no more discontinuity for the different components. In this specific case, the propagating waves are leaky waves whatever the electron density, except for two singular values $n_e = 0$ m^{-3} (*i.e.*, for the empty line), and $n_e \approx 3.08 \times 10^{18}$ m^{-3} for which we rigorously have a pseudo-surface wave since $k'_{y,p}$ is zero.

Finally, we can conclude that the mode of propagation associated with this waveguide departs from a quasi-TEM mode in the low-frequency limit when the cavity is filled with a plasma instead of vacuum.

5. Fundamental mode in the waveguide filled with inhomogeneous plasma

The analysis in Section 4 considered a homogeneous plasma inside the cavity. Practically, the electron density, and thus the relative permittivity, of the plasma are inhomogeneous. One can wonder whether the conclusions drawn above remain valid.

In order to study the coupling between the microwave electromagnetic field and a more realistic plasma discharge, the plasma-based microwave power limiter has also been simulated with a 2D self-consistent numerical model [11]. The numerical results allow us to first investigate how the wave is coupled to the plasma by analyzing the Poynting vector. Secondly, the data obtained from the numerical model (electron density and electromagnetic field mapping) are used as input data for the analytical model, enabling us to conclude on the wave's propagation modes.

‡ In this work we choose to define the critical density as the density for which $\varepsilon'_{r,p} = 0$, that is to say

$$n_c = \frac{m_e \varepsilon_0}{e^2}(\omega^2 + \nu_m^2) \tag{21}$$

Note however that it is only rigorously defined for non-collisional plasma.

5.1. Poynting vector

Figure 10 shows the simulated steady-state Poynting vector lines as well as the electron density map within the microwave power limiter for an input power of 10 W at 3 GHz. The microstrip line and the ground plane carrying the microwave signal are at $y = 0.508$ mm and $y = -1.524$ mm, respectively. The dotted black line marks the interface between the dielectric slab, in the upper region, and the cavity filled with plasma, in the lower region. The red line at $x = 10$ mm represents the location of the current sheet that generates the incident electromagnetic field. Note that the gas-filled cavity starts at $x = 20$ mm and that the MHCD source is located at $x = 70$ mm.

From Poynting vector lines, we can see that, if one part of the microwave incident power is reflected because of impedance mismatching, a large part of this power partly bypasses the head of the steady-state plasma column through the dielectric slab. It clearly highlights the role of the dielectric slab in supplying power to this microwave-sustained plasma discharge.

This result can also be justified analytically. If we assume that the propagation constant can be written as a function of an effective permittivity $\underline{\varepsilon}_r$ such that $\underline{k}_x = k_0\sqrt{\underline{\varepsilon}_r}$, this complex effective permittivity can be

deduced from equation (15) as

$$\varepsilon'_r = \frac{\varepsilon'_{r,p} + \frac{\varepsilon'^2_{r,p}+\varepsilon''^2_{r,p}}{\underline{\varepsilon}_{r,d}} \frac{l_d}{l_p}}{\left(1 + \frac{\varepsilon'_{r,p}}{\varepsilon'_{r,d}} \frac{l_d}{l_p}\right)^2 + \frac{\varepsilon''^2_{r,p}}{\varepsilon'^2_{r,d}} \frac{l_d^2}{l_p^2}} \left(1 + \frac{l_d}{l_p}\right) \quad (22)$$

$$\varepsilon''_r = \frac{\varepsilon''_{r,p}}{\left(1 + \frac{\varepsilon'_{r,p}}{\varepsilon'_{r,d}} \frac{l_d}{l_p}\right)^2 + \frac{\varepsilon''^2_{r,p}}{\varepsilon'^2_{r,d}} \frac{l_d^2}{l_p^2}} \left(1 + \frac{l_d}{l_p}\right) \quad (23)$$

Since the real and imaginary parts of the propagation constant are defined as

$$k'_x = k_0 \sqrt{\frac{|\underline{\varepsilon}_r| + \varepsilon'_r}{2}} \quad (24)$$

$$k''_x = k_0 \sqrt{\frac{|\underline{\varepsilon}_r| - \varepsilon'_r}{2}} \quad (25)$$

whatever the medium, one deduces that if the plasma absorbs the microwave power (*i.e.*, $\varepsilon''_{r,p} \neq 0$), then $k''_x \neq 0$ and the electromagnetic field decays both in the plasma and the dielectric slab as it propagates along the x-direction. This is also observed on the evolution of the magnitude of the Poynting vector in figure 10. Since the dielectric slab is supposed to be lossless both in simulation and in analytical calculations, the decrease of the magnitude of the field in the dielectric slab can only been explained by a transfer of the microwave power from the slab to the plasma. Nevertheless, if this demonstration highlights the role of the dielectric in the power feeding of the plasma discharge, it has to be mentioned that a small amount of power also bypasses the over-dense head of the plasma columns through the sheaths. Moreover, this study in terms of Poynting vector does not allow to conclude on the type of wave that propagates along the waveguide. This can only be performed by extracting the propagation constant in the simulation results, and thereby calculating the wave vectors in the plasma region. This is the subject of the next section.

5.2. Propagation constant

Historically, the first measurement of electron densities in surface wave sustained discharges was performed by Zakrzewski *et al.*, by measuring the real and imaginary parts of the propagation constant through interferometry methods [26, 27]. Their procedure can be summarized as follows.

- First, they measured either the phase shift induced by the electron density for a non-collisional plasma, or the attenuation of the electric field for the wave travelling along a collisional plasma column. These two quantities have been expressed in terms of the real part and of the imaginary parts of the propagation constant.

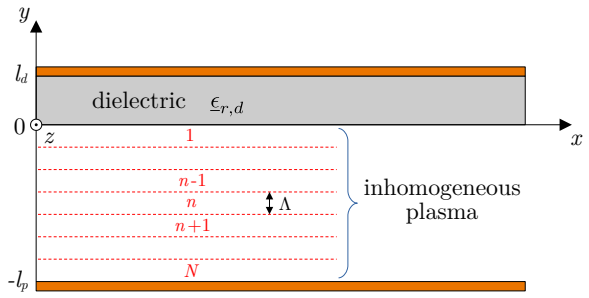

Figure 11. Schematic of the plasma-based microwave power limiter with a non-uniform plasma along the y-direction. The electron density remains invariant in the x-direction.

- Then, they calculated analytically the electromagnetic field within their plasma column for an axial uniform electron density, which leads to a transcendental equation from which the dispersion relation for the microwave field can be obtained.
- Finally, by assuming that the experimental microwave field in the plasma column takes locally the same form as that given by the solution of Maxwell's equations, they got the electron density from the dispersion relation [28].

In our case, the electron density and electromagnetic field are known from the simulation, and we can use them as input data in our theoretical model to obtain the propagation constant by assuming that the dispersion relation is locally verified. However, the analytical developments conducted in Section 4 have been made considering a homogeneous electron density in the cavity, and we can observe from the simulated results in figure 10 that it is inhomogeneous in both x- and y-directions. As a consequence, it is required to extend the computation of the electromagnetic field considering this 2D electron density profile.

The analytical model developed in Section 2.3 has thus been extended to take into account this inhomogeneous plasma. To do so, the plasma is subdivided into N layers of thickness $\Lambda = l_p/N$ along the y-direction as shown in figure 11. The analytical solution of this multilayer problem can be obtained by following the same procedure described in Section 2.3. For sake of brevity, the developments are not described here, but helpful information such as the expressions of the electromagnetic fields, the transcendental equation, and a study of convergence on the number of layers can be found in Appendix B.

One can finally extract the simulated value of the E_d^y component at the boundary between the dielectric slab and the plasma and compute the wave vectors. Note that the plasma discharge has been here discretized into $N = 105$ layers. Indeed, a convergence

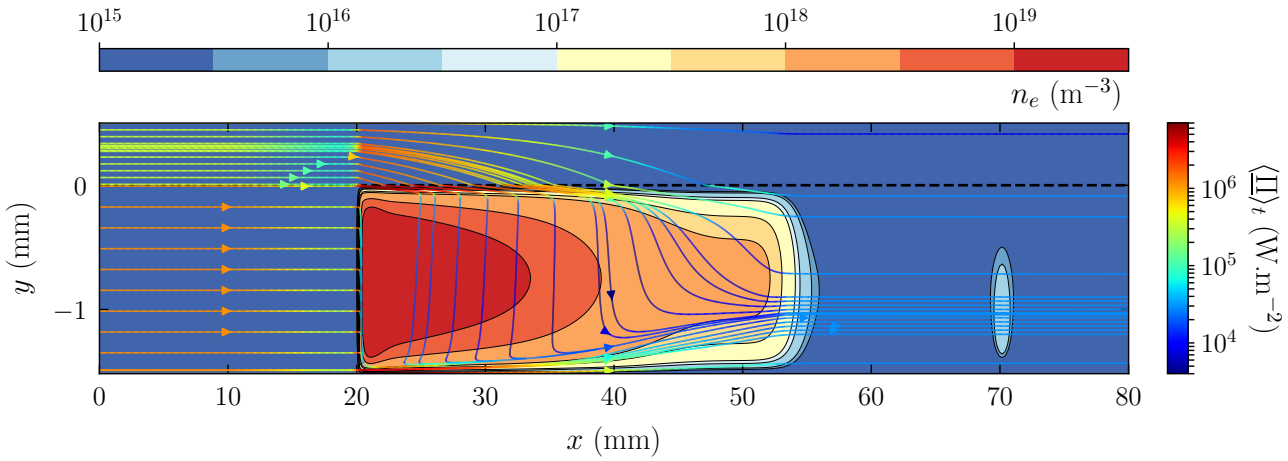

Figure 12. Computed time-average Poynting vector lines and simulated electron density for a steady-state plasma with an incident power of 10 W at 3 GHz. The dotted black line marks the boundary between the dielectric slab and the plasma.

study has shown that a number of layers $N \geqslant 100$, is sufficient to limit the error on the propagation constant to less than 1%. These computations have been repeated all along the x-direction in order to take into account the longitudinal variation of the electron density shown in figure 10. Finally, the computed Poynting vector map is shown in figure 12. As we can see, there is a good agreement in terms of the norm of the Poynting vector and the direction of the power flow. However, this method does not describe the power propagation in the head of the plasma column where the electron density strongly increases as a function of x. An advanced mode matching technique is required to take into account the low-order mode and a large number of localized modes. These localized modes are modes for which the imaginary part of the propagation constant is higher than the real part, and which decrease rapidly as one moves away from the front.

The propagation constant is then computed using the simulated results and the analytical transcendental equation so that we obtain the $k'_{y,p}$ component of the wave vector in the plasma region as a function of y for several maximum densities. The algebraic angle θ that the real part of the wave vector makes with the x-axis, can finally be obtained from

$$\theta = \arctan\left(\frac{k'_{y,p}}{k'_x}\right) \tag{26}$$

As mentioned previously, if $k'_{y,p}/k'_x \ll 1$, the wave vector is nearly parallel to the interface between the dielectric slab and the plasma, and we then have a pseudo-surface wave. If not, the wave at the interface behaves as a leaky-wave.

Figure 13 presents the profiles of the $k'_{y,p}$ values normalized to the real part of the propagation constant

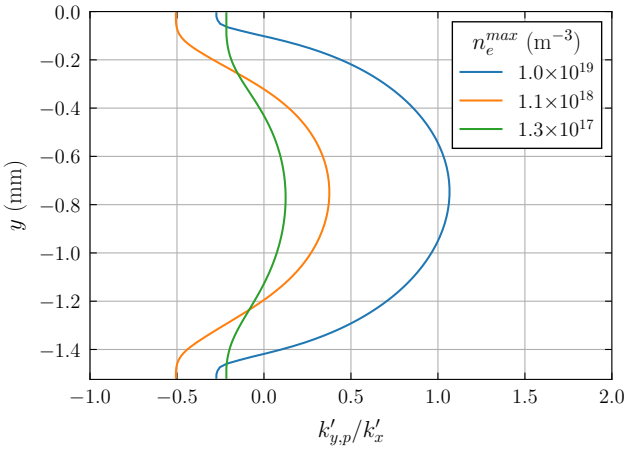

Figure 13. Computed $k'_{y,p}$ component of the wave vector in the plasma simulation domain for several positions along the column, that is to say several maximum densities.

k'_x. For high values of the maximum electron density, the ratio $k'_{y,p}/k'_x$ is far different of zero, and we have a leaky-wave. When the maximum electron density decreases (*i.e.*, near the end of the plasma column), the mode turns back to the fundamental mode described in Section 3.1 for the empty waveguide, that is to say a pseudo-surface wave.

6. Conclusion

A plasma-based microwave power limiter has recently been proposed in a suspended microstrip technology and designed to work in argon at 10 Torr with a frequency of 3 GHz. An analytical study has been proposed in order to qualify the microwave/plasma coupling, by assimilating the limiter to an inho-

mogeneously dielectric filled parallel-plate waveguide. Maxwell's equations were thus solved in a 2D approximation in order to get the expressions of the electromagnetic fields. The expression for the propagation constant was deduced from the transcendental equation that comes from the field matching at the boundary between the dielectric slab and the plasma.

A modal analysis of the empty line allows to identify the different types of propagation both in terms of wave vectors and electric field magnitude variations. The low order mode at 3 GHz in the empty line was identified as a pseudo-surface wave, for which the wavevector in the cavity is colinear to the dielectric interface.

The modal analysis was extended to the case of a cavity filled with uniform electron density. In the case of a non-collisional plasma, for high values of electron density, the so-called surface plasmon or pure surface wave, for which the wave vector is along the boundary both in the plasma and dielectric slab, takes place in the line. This mode is the same one used for a long time in the surface wave sustained discharges. For low electron densities, a cut-off regime is observed for which the signal can no more propagate in the line. In the limit of highly collisional plasmas, such as for our operating conditions, the cut-off regime disappears and the electromagnetic wave is a leaky wave whatever the density of the plasma.

Finally, we studied the microwave propagation considering a cavity filled with a non-uniform plasma column obtained from a 2D self-consistent simulation. The analytical dispersion relation was extended for the case of a non-uniform plasma, and the measurements of the propagation constant confirmed that the discharge is sustained by a leaky wave in the condition of operation we are interested in. Furthermore, the analysis of the simulated Poynting vector map shows how the electromagnetic power carried in the dielectric slab is transferred to the discharge as the wave propagates along the plasma column. This result has also been demonstrated and illustrated with the analytical developments, and is the consequence of the necessary field matching at the boundary of the dielectric slab.

These results and formulas will be used in further studies, to give a better understanding of the mechanisms involved in the microwave power limitation and to identify ways of optimizing the protection device.

Acknowledgments

The authors would like to thank the Délégation Générale pour l'Armement (DGA), the Agence de l'Innovation de Défense (AID), the Région Occitanie Pyrénées-Méditerranée and the Agence Nationale de la Recherche (ANR-21-ASM1-0002) for their financial support.

Appendix A. Demonstration of the Snell-Descartes's law in the empty line

Figure A1 represents a zoom of figure 6 for the frequency of 85 GHz, on which the angle of incidence i_d of the ray in the dielectric and the angle of refraction i_p of the ray in the cavity are indicated.

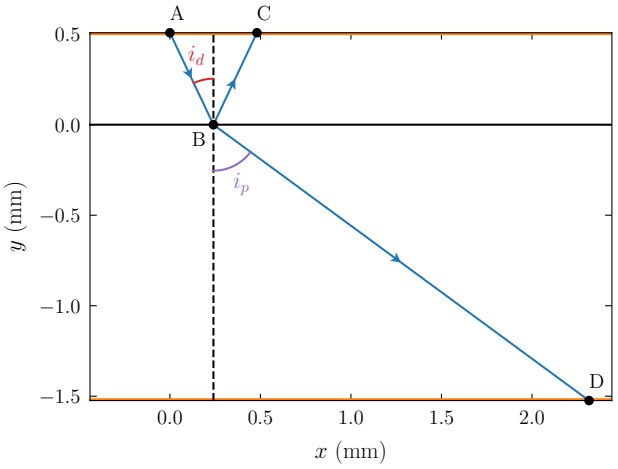

Figure A1. Schematic showing the fate of a light beam as it passes through the dielectric/vacuum dioptre at a frequency $f = 85$ GHz. The surface normal is represented by the dotted black line. The angles of incidence and refraction are i_d and i_p, respectively.

Whatever the medium m considered, the angle i_m verifies the trigonometric relationship

$$i_m = \arctan\left(\frac{\underline{k}_x}{\underline{k}_{y,m}}\right) \tag{A.1}$$

and since

$$\sin\left(\arctan\left(x\right)\right) = \frac{x}{\sqrt{x^2+1}} \tag{A.2}$$

we have

$$n_m \sin(i_m) = \frac{n_m}{\sqrt{\underline{k}_x^2 + \underline{k}_{y,m}^2}}\underline{k}_x = \frac{\underline{k}_x}{k_0} \tag{A.3}$$

where n_m is the relative index of the media m defined as $n_m = \sqrt{\underline{\varepsilon}_{r,m}}$. Since $\underline{k}_x$ has the same value in both the dielectric and the plasma, the above equation leads to the so-called Snell–Descartes laws of geometrical optics

$$n_d \sin(i_d) = n_p \sin(i_p) \tag{A.4}$$

If the cavity is empty, the plasma dielectric constant $\underline{\varepsilon}_{r,p}$ is equal to 1, as well as the refractive

index n_p. Thus, equation (A.3) leads to the expression of the angle of refraction in the cavity

$$i_p = \arcsin\left(\frac{\underline{k}_x}{k_0}\right) \tag{A.5}$$

Appendix B. Formulas for a 2D waveguide filled with non-uniform plasma

Appendix B.1. Solution of Maxwell's equations

The field in the dielectric part is given by

$$\underline{E}_d^x(x,y) = \underline{E}_{d,p}\frac{\sin(\underline{k}_{y,d}[l_d-y])}{\sin(\underline{k}_{y,d}l_d)}\mathrm{e}^{i\underline{k}_x x} \tag{B.1}$$

$$\underline{E}_d^y(x,y) = -i\underline{E}_{d,p}\frac{\underline{k}_x}{\underline{k}_{y,d}}\frac{\cos(\underline{k}_{y,d}[l_d-y])}{\sin(\underline{k}_{y,d}l_d)}\mathrm{e}^{i\underline{k}_x x} \tag{B.2}$$

$$\underline{B}_d^z(x,y) = -i\underline{E}_{d,p}\frac{k_0^2\underline{\varepsilon}_{r,d}}{\omega\underline{k}_{y,d}}\frac{\cos(\underline{k}_{y,d}[l_d-y])}{\sin(\underline{k}_{y,d}l_d)}\mathrm{e}^{i\underline{k}_x x} \tag{B.3}$$

and the field in the layer n writes

$$\underline{E}_p^x = \left[\underline{E}_p^{n-1/n}\frac{\sin(\underline{k}_{y,p}^{(n)}[y+n\Lambda])}{\sin(\underline{k}_{y,p}^{(n)}\Lambda)} - \underline{E}_p^{n/n+1}\frac{\sin(\underline{k}_{y,p}^{(n)}[y+(n-1)\Lambda])}{\sin(\underline{k}_{y,p}^{(n)}\Lambda)}\right]\mathrm{e}^{i\underline{k}_x x} \tag{B.4}$$

$$\underline{E}_p^y = i\frac{\underline{k}_x}{\underline{k}_{y,p}^{(n)}}\left[\underline{E}_p^{n-1/n}\frac{\cos(\underline{k}_{y,p}^{(n)}[y+n\Lambda])}{\sin(\underline{k}_{y,p}^{(n)}\Lambda)} - \underline{E}_p^{n/n+1}\frac{\cos(\underline{k}_{y,p}^{(n)}[y+(n-1)\Lambda])}{\sin(\underline{k}_{y,p}^{(n)}\Lambda)}\right]\mathrm{e}^{i\underline{k}_x x} \tag{B.5}$$

$$\underline{B}_p^z = i\frac{k_0^2\underline{\varepsilon}_{r,p}^{(n)}}{\omega\underline{k}_{y,p}^{(n)}}\left[\underline{E}_p^{n-1/n}\frac{\cos(\underline{k}_{y,p}^{(n)}[y+n\Lambda])}{\sin(\underline{k}_{y,p}^{(n)}\Lambda)} - \underline{E}_p^{n/n+1}\frac{\cos(\underline{k}_{y,p}^{(n)}[y+(n-1)\Lambda])}{\sin(\underline{k}_{y,p}^{(n)}\Lambda)}\right]\mathrm{e}^{i\underline{k}_x x} \tag{B.6}$$

and where $\underline{E}_p^{n-1/n}$ (resp. $\underline{E}_p^{n/n+1}$) is the magnitude of the field at the interface between the layers $n-1$ and n (resp. n and $n+1$). The transcendental equation is obtained by matching the magnetic field components on every interfaces, that leads to the relation

$$\left[\alpha_p^{(N-1)} + \alpha_p^{(N)}\right]A_{N-1} - \frac{A_{N-2}}{\beta_p^{(N-1)}} = 0 \tag{B.7}$$

with

$$\alpha_p^{(n)} = \frac{\underline{\varepsilon}_{r,p}^{(n)}}{\underline{k}_{y,p}^{(n)}}\operatorname{cotan}(\underline{k}_{y,p}^{(n)}\Lambda) \tag{B.8}$$

$$\beta_p^{(n)} = \frac{\underline{k}_{y,p}^{(n)}}{\underline{\varepsilon}_{r,p}^{(n)}}\sin(\underline{k}_{y,p}^{(n)}\Lambda) \tag{B.9}$$

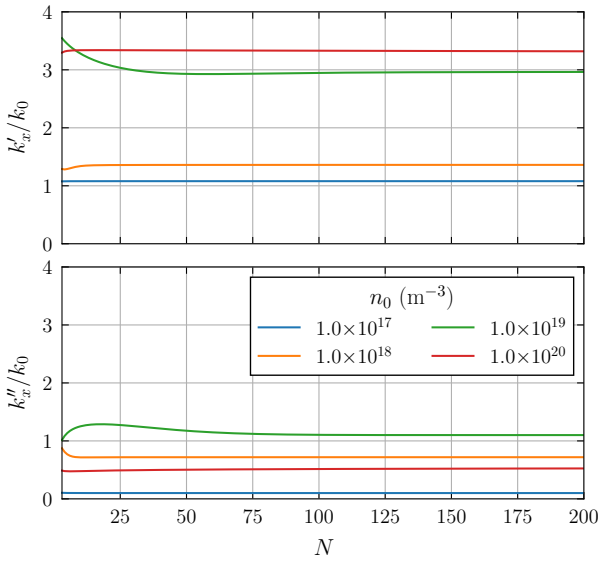

Figure B1. Evolution of the real and imaginary parts of the propagation constant as a function of the number N of layers in the plasma, for several maximum densities.

and where $A_n = \underline{E}_p^{n/n+1}/\underline{E}_{d,p}$ satisfies the following recurrence relation

$$\begin{aligned} A_0 &= 1 \\ A_1 &= \left[\frac{\underline{\varepsilon}_{r,d}}{\underline{k}_{y,d}}\operatorname{cotan}(\underline{k}_{y,d}l_d) + \alpha_p^{(1)}\right]\beta_p^{(1)} \\ A_{n+1} &= \left(\left[\alpha_p^{(n)} + \alpha_p^{(n+1)}\right]A_n - \frac{A_{n-1}}{\beta_p^{(n)}}\right)\beta_p^{(n+1)} \end{aligned} \tag{B.10}$$

Appendix B.2. Convergence study

In order to determine the minimum number N of layers to represent the inhomogeneous plasma, we assume an electron density profile of the form [29]

$$n_e(y) = -4n_0\left(\frac{y^2}{l_p^2} + \frac{y}{l_p}\right) \tag{B.11}$$

This profile is fairly representative of that obtained in simulation for densities typically higher than the critical density. Figure B1 shows the evolution of the real and imaginary parts of the propagation constant of the fundamental mode as a function of the number of layers N and for several maximum densities n_0. It appears that a number of layers $N \geqslant 100$ is sufficient to limit the error to less than 1 %.

References

[1] Ferreira C M and Moisan M 1993 *Microwave Discharges, Fundamentals and Applications* (NATO ASI Series)

[2] Tiwari S, Caiola A, Bai X, Lalsare A and Hu J 2020 *Plasma Chem. Plasma Process.* **40** 1–23
[3] Lebedev Y A 2015 *Plasma Sources Sci. Technol.* **24** 053001
[4] Fehsenfeld F C, Evenson K M and Broida H P 1965 *Rev. Sci. Instrum.* **36** 294–298
[5] Trivelpiece A W and Gould R W 1959 *J. Appl. Phys.* **30** 1784–1793
[6] Moisan M, Beaudry C and Leprince P 1974 *Phys. Lett. A* **50** 125–126
[7] Moisan M, Beaudry C and Leprince P 1975 *IEEE Trans. Plasma Sci.* **3** 55–59
[8] Komachi K and Kobayashi S 1989 *J. Microw. Power Electromagn. Energy* **24** 140–149
[9] Komachi K 1993 *J. Vac. Sci. Technol. A* **11** 164–167
[10] Komachi K 1994 *J. Vac. Sci. Technol. A* **12** 769–771
[11] Fuster L, Hagelaar G, Pascaud R, Simon A, Hoffmann P, Liard L, Pascal O and Callegari T 2022 *Plasma Sources Sci. Technol.* **31** 025009
[12] Schelkunoff S 1959 *IRE Trans. Antennas Propag.* **7** 133–139
[13] Rider A E, Ostrikov K and Furman S A 2012 *Eur. Phys. J. D* **66** 226–245
[14] Balosso O, Sokoloff J and Bolioli S 2012 Brief overview about surface wave theory and applications *2012 15 International Symposium on Antenna Technology and Applied Electromagnetics* pp 1–7
[15] Moisan M, Shivarova A and Trivelpiece A W 1982 *Plasma Phys.* **24** 1331
[16] Shivarova A and Zhelyazkov I 1978 *Plasma Phys.* **20** 1049
[17] Moisan M and Pelletier J 1992 *Microwave Excited Plasmas* (Elsevier)
[18] Lieberman M A and Lichtenberg A J 2005 *Principles of Plasma Discharges and Materials Processing* (Wiley)
[19] Collin R E and Zucker F J 1969 *Antenna theory - Part 2* (McGraw-Hill)
[20] Sihvola A, Jiaran Q and Lindell I V 2010 *IEEE Antennas Propag. Mag.* **52** 124–136
[21] Collin R E 2001 *Foundations for Microwave Engineering, Second Edition* (Wiley-IEEE Press)
[22] Collin R E 1991 *Field Theory of Guided Waves, Second Edition* (Wiley-IEEE Press)
[23] Harrington R F 2001 *Time-Harmonic Electromagnetic Fields* (Wiley-Interscience)
[24] Jenkins F A and White H E 1976 *Fundamental of Optics, Fourth Edition* (McGraw-Hill)
[25] Raizer Y P 1991 *Gas Discharge Physics* (Springer Berlin)
[26] Zakrzewski Z, Moisan M, Glaude V M M, Beaudry C and Leprince P 1977 *Plasma Phys.* **19** 77
[27] Chaker M, Nghiem P, Bloyet E, Leprince P and Marec J 1982 *J. Physique Lett.* **43** 71–75
[28] Glaude V M M, Moisan M, Pantel R, Leprince P and Marec J 2008 *J. Appl. Phys.* **51** 5693–5698
[29] Trivelpiece A W 1958 *Slow wave propagation in plasma waveguides.* Ph.D. thesis California Institute of Technology